ACCEPTED MANUSCRIPT

Journal of Vacuum Science & Technology A

This is the author's peer reviewed, accepted manuscript. However, the online version of record will be different from this version once it has been copyedited and typeset.
PLEASE CITE THIS ARTICLE AS DOI: 10.1116/6.0002987

Band-Engineered $LaFeO_3$-$LaNiO_3$ Thin Film Interfaces for Electrocatalysis of Water

Running title: Band-Engineered $LaFeO_3$-$LaNiO_3$

Running Authors: Paudel et al.

Rajendra Paudel[1], Andricus R. Burton[2], Marcelo A. Kuroda[1], Byron H. Farnum[2], and Ryan B. Comes[1a]
[1] Department of Physics, Auburn University, Auburn, AL 36849 USA
[2] Department of Chemistry and Biochemistry, Auburn University, Auburn, AL 36849 USA

[a)] Electronic mail: ryan.comes@auburn.edu

Iron and nickel-based perovskite oxides have proven promising for the oxygen evolution reaction (OER) in alkaline environments, as their catalytic over-potentials rivaling precious metal catalysts when the band alignment is tuned through substitutional doping or alloying. Here we report the engineering of band alignment in $LaFeO_3$/$LaNiO_3$ (LFO/LNO) heterostructures via interfacial doping that yields greatly enhanced catalytic performance. The 0.2 eV offset (VBO) between the Fermi level in metallic LNO and the valence band in semiconducting LFO that we predict using density functional theory makes LFO a *p*-type semiconductor results in significantly lower barriers for hole transport through LFO compared to the intrinsic material. Experimental band alignment measured with *in situ* X-ray photoelectron spectroscopy of epitaxial LFO/LNO heterostructures confirm these predictions, producing a measured VBO of 0.3(1) eV. Furthermore, OER catalytic measurements on these samples in alkaline solution show an increase in catalytic current density by a factor of ~275 compared to LFO grown on *n*-type Nb-doped $SrTiO_3$. These results demonstrate the power of tuning band alignments through interfacial band engineering for improved catalytic performance of oxides.

ACCEPTED MANUSCRIPT

Journal of Vacuum Science & Technology A

This is the author's peer reviewed, accepted manuscript. However, the online version of record will be different from this version once it has been copyedited and typeset.
PLEASE CITE THIS ARTICLE AS DOI: 10.1116/6.0002987

I. INTRODUCTION

Interfaces in complex oxide thin film heterostructures are particularly interesting because of their non-equilibrium electronic properties, which usually do not exist in the bulk or even in uniform films. These unique properties emerge as a result of interfacial interactions, such as an offset in the band alignment for occupied states accompanied by charge transfer across the interface[1–12]. The band gap of the materials[13], separation between O 2p and metal 3d states[14], and film thickness[15] all play a significant role in charge transfer at the interfaces and band alignment at the surface. Careful epitaxial growth by molecular beam epitaxy or pulsed laser deposition enables control of these parameters individually and offers a route to the rational development of new functional materials for applications in renewable energy systems.

Transition metal (TM) oxide thin films, heterostructures, and interfaces have emerged as ideal model systems for understanding catalysis in energy conversion devices (electrochemical cells) by splitting of water via the oxygen evolution reaction (OER) and hydrogen evolution reaction (HER)[16–18]. The available descriptors for high OER activity are based on the number of TM 3d (e_g) electrons[19], the extent of O 2p-TM 3d bonding hybridization, the valence state of TM[20], and oxygen binding energy at the surface[21,22]. These parameters can be tuned by controlled doping on the perovskite A and B sites and creating interfaces and heterostructures[18,23–27]. Collectively, these effects tune the alignment of TM 3d electronic states relative to both the Fermi level and the OER reaction potential energy, which can reduce overpotentials for electrocatalysis.

$LaNiO_3$ (LNO) and other perovskite nickelates have been reported to exhibit excellent catalytic performance for OER[18,28]. Bak et al. have shown that perturbing NiO_6

ACCEPTED MANUSCRIPT
Journal of Vacuum Science & Technology A
This is the author's peer reviewed, accepted manuscript. However, the online version of record will be different from this version once it has been copyedited and typeset.
PLEASE CITE THIS ARTICLE AS DOI: 10.1116/6.0002987

octahedra by electrochemical exchange of Fe on the LNO surface facilitates charge transfer and improves OER activity[29]. Similar results have been reported by doping Fe on the B-site to generate partial electron transfer from Fe to Ni, leading to an $Fe^{3+\delta}$ and $Ni^{3-\delta}$ formal charge[24]. These alloy $La(Fe,Ni)O_3$ materials exhibited greater electrocatalytic performance than either pure $LaFeO_3$ (LFO) or LNO [24]. Partial oxidation of Fe^{3+} results in stronger hybridization between O 2p and Fe 3d orbitals, which increases covalency and results in higher OER activity of the perovskites[19,20]. Others have also shown that Fe dopants into LNO films can enhance catalytic performance by roughly a factor of 2 compared to pure LNO through engineering of conductivity and tuning the density of states for 3d electrons near the Fermi level[30].

The extrinsic doping required for catalytic enhancement may alternatively be attained by engineering the band alignments in LNO heterostructures that avoid disorder introduced by impurity atoms. To this end, LFO/LNO heterostructures might push boundaries in OER performance as $LaFeO_3$ (LFO) is itself a good candidate for OER catalysis, particularly when hole doped [15,31], and given its electronic structure, LFO/LNO heterostructures might push boundaries in OER performance through interfacial hole doping of LFO. However, the LFO/LNO interface is noticeably lacking in exploration, both experimentally and theoretically.

In this work we characterize the band alignment and catalytic performance of LFO/LNO heterostructures grown using molecular beam epitaxy (MBE). Band alignment and charge transfer at the LFO/LNO interface is studied via both first-principles calculations and *in situ* X-ray photoelectron spectroscopy (XPS)[32]. First-principles density functional theory (DFT) are compared to predictions based on the valence states formed by oxygen[14] and XPS studies on epitaxial LFO/LNO heterostructures. Moreover, these LFO/LNO

ACCEPTED MANUSCRIPT

Journal of Vacuum Science & Technology A

This is the author's peer reviewed, accepted manuscript. However, the online version of record will be different from this version once it has been copyedited and typeset.
PLEASE CITE THIS ARTICLE AS DOI: 10.1116/6.0002987

heterostructures show an increase in OER catalytic reaction rate by over two orders of magnitude via cyclic voltammetry measurements compared to LFO films grown directly on *n*-doped $SrTiO_3$[15]. By turning an intrinsic semiconductor into a non-degenerate *p*-type material, this work demonstrates that band engineering of these epitaxial LFO thin films can attain significant enhancements in catalytic performance.

II. EXPERIMENTAL AND COMPUTATIONAL METHODS

A. DFT calculations

Computational descriptions of these heterostructures were carried out on a $LaFeO_3/LaNiO_3$ superlattice comprised of 4 layers of each material with a $\sqrt{2}\times\sqrt{2}$ in-plane configuration assuming periodic boundary conditions in all directions. G-type antiferromagnetic polarization for LFO [33] and no spin polarization in LNO were used to replicate the magnetic behavior of each material at room temperature[34]. In-plane lattice constants were constrained to match the lattice parameter of LFO, and equilibrium lattice parameters along out-of-plane directions and atomic coordinates were obtained by relaxation of the superlattice. Projector augmented wave (PAW)[35] pseudopotentials were used for the description of the atomic cores along with the generalized gradient approximation (GGA) of Perdew-Burke-Ernzerhorf (PBE)[36] for the exchange-correlation functional. Calculations also included corrections based on the Hubbard model[37] to improve the ground state description and correct the band gap of these highly correlated electron systems[38]. The Hubbard *U* parameters for Fe (U_{Fe} = 2.84 eV), Ni (U_{Ni} = 3.05 eV), and O (U_O = 6.34 eV) reproduced the experimental band gap in the bulk LFO and LNO as previously reported in the literature[38] and were employed for heterostructure calculations. (Comparison with cases where the Hubbard correction is applied only to the

ACCEPTED MANUSCRIPT
Journal of Vacuum Science & Technology A
This is the author's peer reviewed, accepted manuscript. However, the online version of record will be different from this version once it has been copyedited and typeset.
PLEASE CITE THIS ARTICLE AS DOI: 10.1116/6.0002987

3d TM elements is presented in the Supplemental Information.) Energy cut-offs were set to 80 Ry and 600 Ry for wave functions and charge density, respectively. The energy convergence threshold was set to 10^{-6} eV and integration over the superlattice Brillouin zone was performed using an 8×8×1 Monkhorst-Pack *k*-grid[39]. Our first-principles calculations were performed using Quantum Espresso (QE) software suite [40].

B. Synthesis and Characterization

We synthesized epitaxial thin film heterostructures using oxide molecular beam epitaxy (MBE, Mantis Deposition). All samples were grown on 10 mm square 0.7% Nb-doped $SrTiO_3$ (STO) substrates (MTI Crystal) that served as a conductive bottom electrode for XPS and catalysis experiments. STO has a cubic lattice parameter of 3.905 Å while pseudocubic lattice parameters of LFO and LNO, obtained from experimental data are 3.93 Å[41] and 3.83 Å[34], respectively. This small lattice mismatch enables coherent growth of strained thin films. Before loading the substrates into the growth chamber, they were cleaned by sonication in acetone and iso-propyl alcohol, and then dried with molecular nitrogen.

For LNO growth, the Nb:STO substrates were heated to 600 °C in oxygen plasma generated by a 300 W-RF plasma source (Mantis Deposition) and kept at the same temperature until completion of the LNO layer. Immediately after, the substrate was heated to 750 °C for the LFO growth. Metallic fluxes were obtained by heating elemental sources in effusion cells to the evaporation or sublimation point. Elemental fluxes were calibrated using a quartz crystal microbalance (QCM). By controlling the individual shutters, LaO and NiO_2/FeO_2 layers were deposited alternately, as described previously[15,42]. The real-time growth was monitored using reflection high energy electron

ACCEPTED MANUSCRIPT
Journal of Vacuum Science & Technology A
This is the author's peer reviewed, accepted manuscript. However, the online version of record will be different from this version once it has been copyedited and typeset.
PLEASE CITE THIS ARTICLE AS DOI: 10.1116/6.0002987

diffraction (RHEED) from the film surface. RHEED exhibited well-defined oscillations in the intensity during the entire growth, confirming the layer-by-layer growth. The oxygen pressure in the chamber during LNO growth was ~5×10^{-5} Torr with the plasma activated to maximize oxidation of the LNO film. LFO was grown at ~6×10^{-6} Torr in plasma as well. After growth, the samples were cooled in oxygen plasma to room temperature.

Chemical composition and electronic valence state of synthesized samples were established using an appended XPS system (PHI 5400, refurbished by RBD Instruments) furnished with a monochromatic Al Kα X-ray source and pass energy of 17.9 eV. The absolute core level positions cannot be referenced to the Fermi level of the system owing to a electron flood gun used to mitigate charging. Thus, XPS analysis was performed by aligning O 1s peak to 530eV to provide a consistent reference for all spectra. Band alignment measurements were performed via XPS using the Fe 3p and Ni 3p core level spectra, as described previously[1,32,43–45]. Briefly, this method is based on a linear extrapolation of the valence band maximum (VBM) of uniform LFO and LNO films to determine the energy separation between the Fe 3p (Ni 3p) and LFO (LNO) VBM [45]. This separation in energy for each constituent material is taken to be constant when a heterostructure is grown, such that the difference in energy between a specific peak in the Fe 3p and Ni 3p spectra for the heterostructure can be used as a proxy to determine the offset between the valence band maximum of LFO and the Fermi level that is pinned by LNO for the materials at the heterojunction. This analysis is not affected by the electron flood gun as it depends on the relative energy separation of the two core level spectra rather than the absolute binding energy as referenced to the Fermi level[44]. Propagation of

ACCEPTED MANUSCRIPT
Journal of Vacuum Science & Technology A
This is the author's peer reviewed, accepted manuscript. However, the online version of record will be different from this version once it has been copyedited and typeset.
PLEASE CITE THIS ARTICLE AS DOI: 10.1116/6.0002987

error due to the resolution of the analyzer yields error bars for the band alignment of between 0.1 and 0.2 eV.

C. OER Electrocatalysis

To fabricate electrodes for catalytic studies, the samples were diced using a standard dicing saw to 5mm×5mm pieces. These LFO/LNO MBE films were used as electrodes and connected to a glassy carbon electrode (GC, Pine Instruments) as described in our previous work [15]. A bead of gallium indium eutectic (InGa, Ted Pella #**495425**) was placed on the GC working electrode followed by a ring of silver paint (Sigma-Aldrich). The backside of the STO substrate was then pressed gently into the eutectic/silver paint layer. The eutectic has been shown to form good electrical contacts[46], while the silver paint is both conductive and acts as a mild adhesive to keep the substrate in place. Chemically inert epoxy (Loctite, EA E-60HP) was then used to cover any exposed silver paint and seal the edges of the STO substrate, resulting in a roughly circular area of exposed the LFO/LNO MBE film. Electrode areas were measured by processing a digital photograph of the assembled electrode using ImageJ software.

Cyclic voltammetry (CV) experiments were performed with a Pine WaveDriver 20 bipotentiostat using a three-electrode setup in which all electrodes were in the same cell and unseparated by a membrane or frit, with the exception of the reference frit. The working, reference, and counter electrodes were LFO/LNO, Hg/HgO (0.1 M KOH, Pine Instruments), and platinum wire coil respectively. All measurements were carried out under saturated O_2 conditions in water (18 MΩ, Millipore) with 0.1 M KOH electrolyte while rotating the working electrode at 2000 rpm to remove bubbles from the electrode

ACCEPTED MANUSCRIPT
Journal of Vacuum Science & Technology A
This is the author's peer reviewed, accepted manuscript. However, the online version of record will be different from this version once it has been copyedited and typeset.
PLEASE CITE THIS ARTICLE AS DOI: 10.1116/6.0002987

surface. All potentials were converted from Hg/HgO to RHE using the equation: $E_{RHE} = E_{app} + E_{Hg/HgO} + 0.059*pH$. $E_{Hg/HgO}$ was determined to be 0.1 V vs NHE using $[Fe(CN)_6]^{3-/4-}$ as an external standard ($E_{1/2}$ = 0.36 V vs NHE)[46]. CV experiments with iR compensation were performed by sweeping the potential at 20 mV s^{-1} starting from 0.83 and moving to 2.23 V vs RHE for 25 cycles to equilibrate the electrode surface. The current at 1.6 V was found to drop ~5% over the cycling period, but stabilized to a constant value between 10-25 cycles. The anodic trace of the 25th cycle was used for analysis of electrocatalytic performance for OER. All experiments were performed at room temperature.

III. RESULTS

A. DFT Analysis

For a display equation, We first employ first-principles calculation to establish the band alignment and charge transfer across the LFO/LNO interface and better understand how the heterostructures will function as OER catalysts. Strain and bonding environment may alter the electronic properties significantly between a bulk material and heterostructure, necessitating care to decouple interfacial effects from the structural changes imposed by the superlattice[47]. The interface was modeled employing LFO/LNO superlattice with 4 unit cell thickness for each material, as depicted in Figure 1(a). The electronic structure of the interface is rationalized by projecting Bloch states onto localized atomic orbitals in different layers of the superlattice. This decomposition, shown in Figure 1(b), only contains contributions from Fe, Ni and O orbitals as Bloch states formed with La ones only give small contributions in the vicinity of from Fermi level. The LFO bandgap in the heterostructure is estimated to be ~ 2.2 eV, which is in

ACCEPTED MANUSCRIPT
Journal of Vacuum Science & Technology A
This is the author's peer reviewed, accepted manuscript. However, the online version of record will be different from this version once it has been copyedited and typeset.
PLEASE CITE THIS ARTICLE AS DOI: 10.1116/6.0002987

close agreement with the 2.3 eV experimental band gap reported previously [1,48]. Overall, features of the electronic structure are also similar to those obtained in calculations of bulk LFO and LNO presented in Figure S1 and S2 of the supplemental material. For instance, the bands crossing the Fermi level within the LNO layers are strongly hybridized Ni e_g and O 2p orbital bringing metallic character to the heterostructure. Occupied Fe e_g states form the top of the valence band within the LFO layers and unoccupied t_{2g} states are ~2.2 eV above the LFO valence band maximum, which is consistent with the bulk properties. The LFO valence band maximum is formed of hybridized O 2p and occupied Fe^{3+} e_g states and lies ~0.2 eV below the Fermi level (**Figure S3**).

Results from DFT calculations show that the valence band offset (VBO) of ~ 0.2 eV between the LFO and LNO layers, resulting in the nondegenerate p-doping of the LFO. From this offset, we estimate a hole density in the LFO to be 6.0×10^{16} cm^{-3} induced from the charge transfer. In further analysis of the electronic band structure, we calculate the effective mass of LNO holes of approximately $0.61m_e$ (**Figure S4**). Details can be found in supporting information and hole densities are presented in Table S2. We note that if this DFT model is an accurate representation of the electronic structure of an LFO/LNO heterostructure, no spectroscopic evidence of charge transfer would be expected in core level XPS measurements or other X-ray spectroscopy because hole concentrations would be several orders of magnitude below the sensitivity limit of these techniques.

In general, quantitative prediction of band offsets at complex oxide interfaces using computational methods is challenging due to electron correlations, various

ACCEPTED MANUSCRIPT
Journal of Vacuum Science & Technology A
This is the author's peer reviewed, accepted manuscript. However, the online version of record will be different from this version once it has been copyedited and typeset.
PLEASE CITE THIS ARTICLE AS DOI: 10.1116/6.0002987

magnetic states and symmetry considerations[49]. Nonetheless, results could be anticipated from the bulk calculations following the approach by Zhong and Hansmann[14] based on the equilibration of oxygen states yielding the energy continuity of the O 2p band center—the center of mass of the oxygen partial density of states—across the interface.

In these heterostructures, hole-doping of LFO is expected to emerge as in bulk the O 2p-band center of LNO and LFO reside at approximately 2.20 eV and 2.82 eV below the Fermi level, respectively. Once the interface is formed, O 2p-band centers obtained from orbital projections on different layers tend to align, as shown in Figure 1(b) and listed in Table S1. For each material in the heterostructure we observe small differences in the calculated O 2p band centers (< 0.2 eV) likely attributable to local octahedral tilting and spin configuration variations across the interface that break the symmetry of the structure. The O 2p center difference for the NiO_2 planes in LNO reside nearly 0.15 eV above those of FeO_2 in LFO.

ACCEPTED MANUSCRIPT
Journal of Vacuum Science & Technology A
This is the author's peer reviewed, accepted manuscript. However, the online version of record will be different from this version once it has been copyedited and typeset.
PLEASE CITE THIS ARTICLE AS DOI: 10.1116/6.0002987

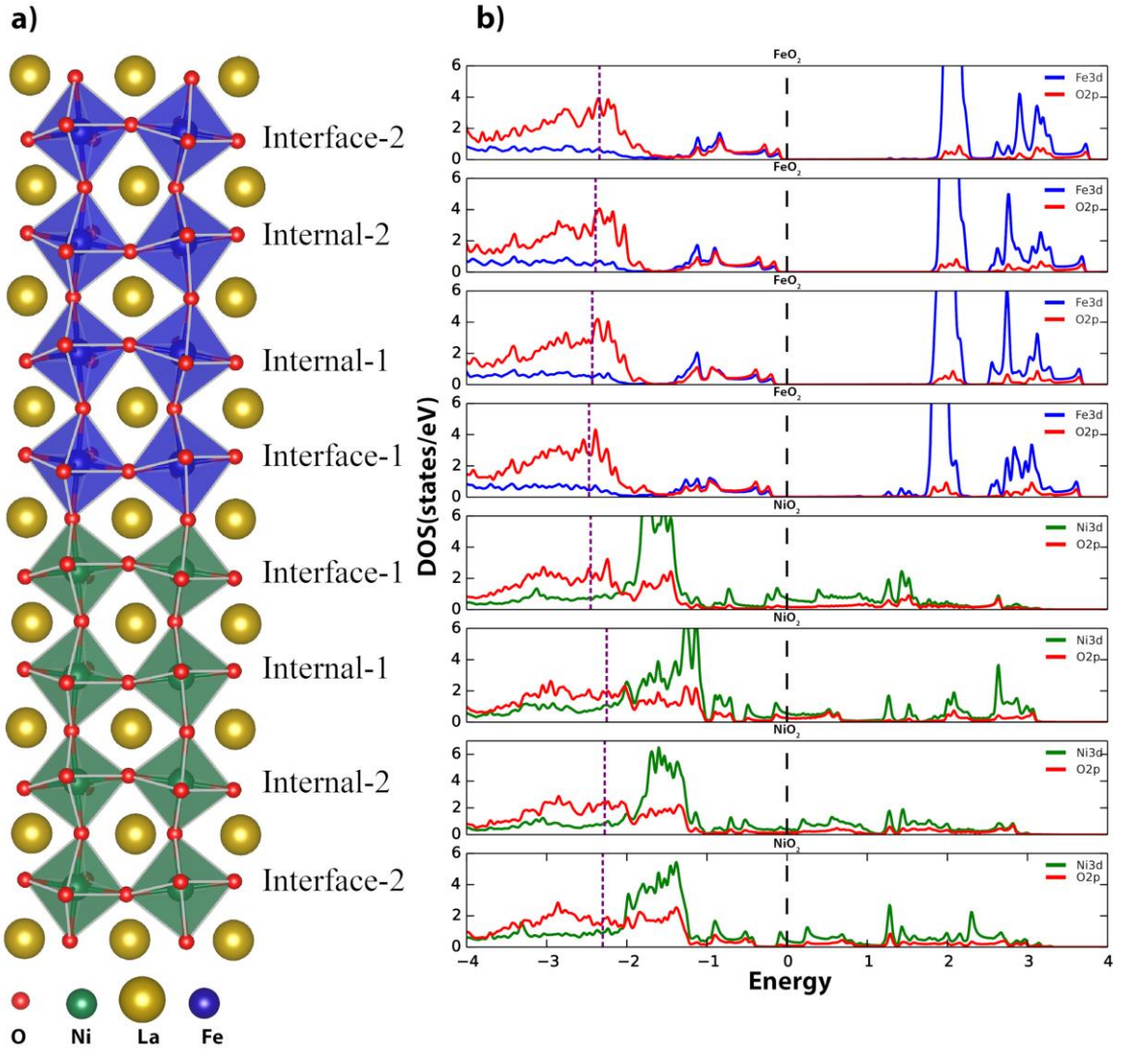

Figure 1: a) LFO/LNO superlattice model used for DFT band alignment predictions; b) Orbital projected density of states projected onto different FeO_2 and NiO_2 layers. Black dashed line is the Fermi energy and green dashed line represents the O 2p band center.

B. *Experimental Band Alignment Studies*

To test the theoretical results determined from DFT, a series of films were grown via MBE and measured using *in situ* XPS[32,43]. This method is based on constant binding energy difference between a chosen core level and the VBM of a material. In ternary complex oxides, accurate theoretical calculation of VBDOS is complicated and

ACCEPTED MANUSCRIPT
Journal of Vacuum Science & Technology A
This is the author's peer reviewed, accepted manuscript. However, the online version of record will be different from this version once it has been copyedited and typeset.
PLEASE CITE THIS ARTICLE AS DOI: 10.1116/6.0002987

computationally expensive[14]. Chambers et. Al proposed a rather simple method of estimating the VBM using extrapolation of the linear part of leading valence band edge to zero level background, which has been found to predict the VBM with sufficient accuracy[45]. Initial LFO and LNO films were grown separately and used as references for determination of the energy difference between core levels and the valence band maximum in each material. These results are shown in Figure 2. The LFO and LNO valence bands extracted from XPS are shown in Figure 2(a-b). Determination of the VBM for LFO and Fermi level location for LNO was performed by extrapolating the linear region of leading valence band edge as shown in the inset. Fits to the Fe 3p and Ni 3p core levels for the same samples are shown in Figure 2(c-d). The lowest binding energy features in each dataset were used to determine the difference in binding energy between the core level and the VBM. Linear extrapolation yields a VBM of LFO at -0.2 eV and the Fermi level location for LNO at -1.1eV. Note that due to the use of the electron flood gun and alignment of the O 1s peak to 530 eV, binding energies are not measured relative to the Fermi level. Because minimal charge transfer is expected across the interface between LNO and LFO, it is safe to conclude that the lowest binding energy features will not change significantly between the uniform films and the heterostructures, which was reflected in the final fits to the peaks for the heterostructures.

ACCEPTED MANUSCRIPT
Journal of Vacuum Science & Technology A
This is the author's peer reviewed, accepted manuscript. However, the online version of record will be different from this version once it has been copyedited and typeset.
PLEASE CITE THIS ARTICLE AS DOI: 10.1116/6.0002987

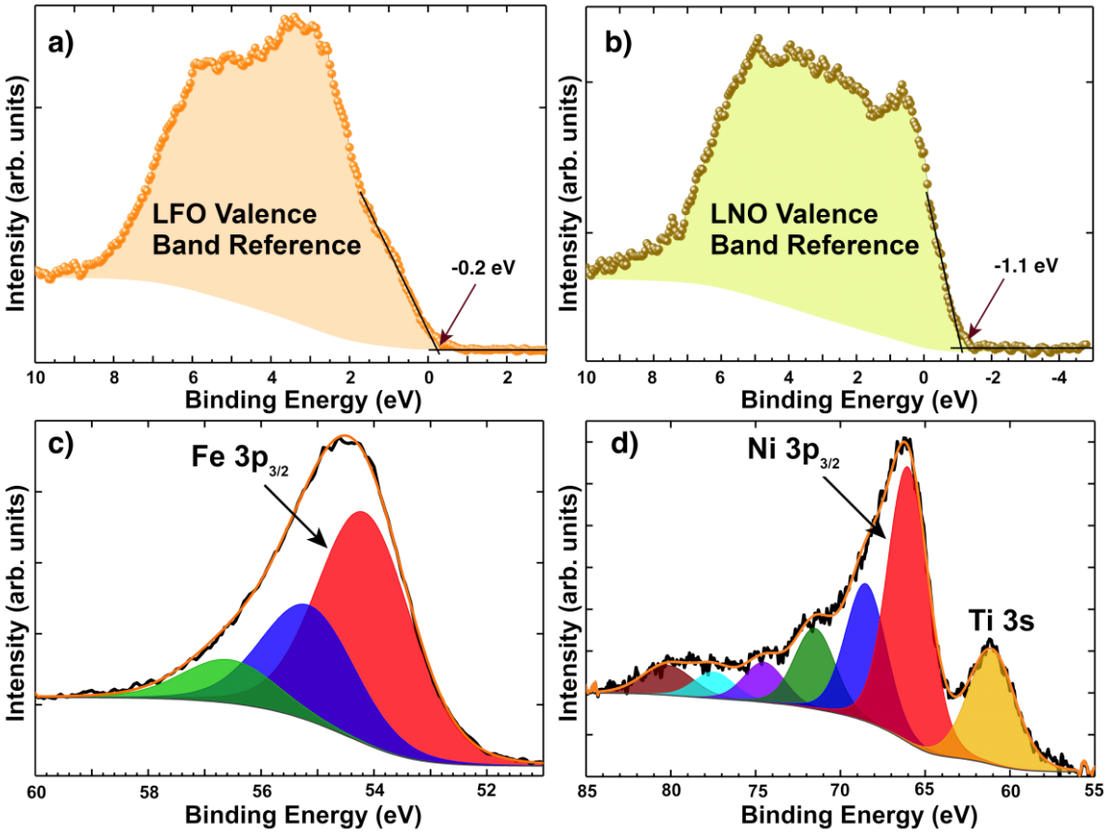

Figure 2: Valence band XPS spectra of a) 6nm thick LFO sample b) 3nm LNO sample and fitting of valence band leading edge using linear extrapolation method c) Fe 3p XPS region of LFO sample d) Ni 3p XPS region for LNO sample.

ACCEPTED MANUSCRIPT
Journal of Vacuum Science & Technology A
This is the author's peer reviewed, accepted manuscript. However, the online version of record will be different from this version once it has been copyedited and typeset.
PLEASE CITE THIS ARTICLE AS DOI: 10.1116/6.0002987

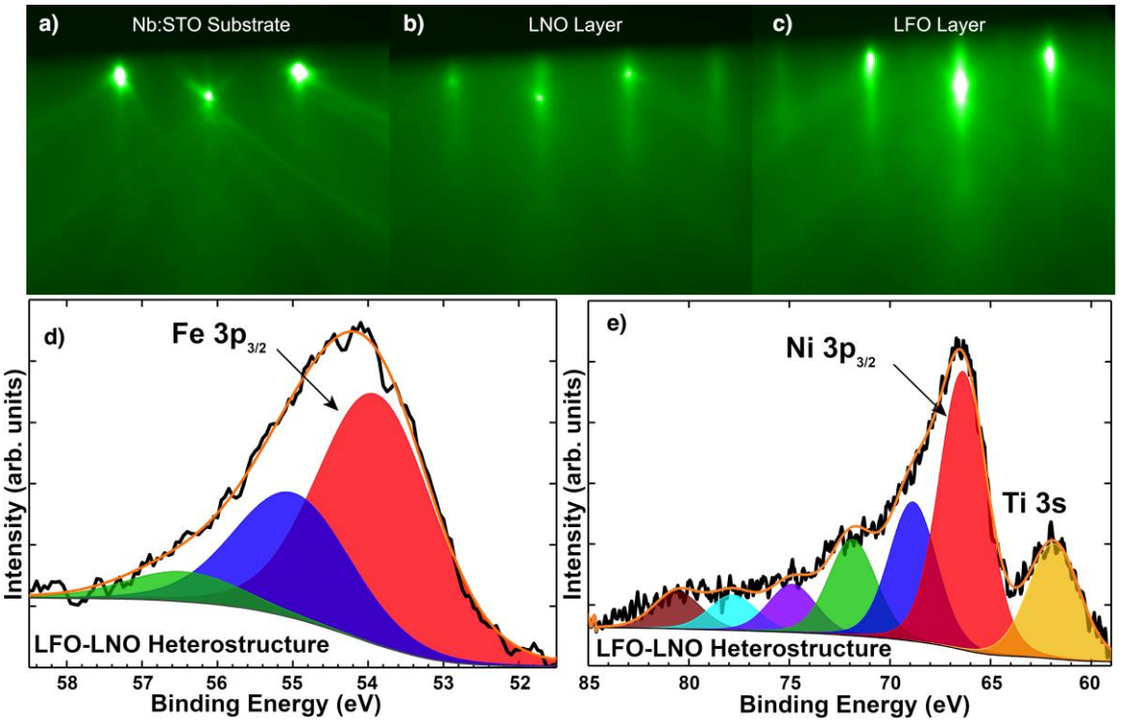

Figure 3: RHEED images of a) Nb:STO substrate b) 4 unit cell LNO-NbSTO c) LFO-LNO-NbSTO with 2 unit cell LFO d)Fe 3p XPS region of LFO-LNO sample-1 e) Ni 3p XPS region of LFO-LNO sample-1

The valence band offset is calculated as

$\Delta E_V = (E_{CL} - E_V)_{LNO} - (E_{CL} - E_V)_{LFO} - \left(E_{CL}^{Ni\ 3p} - E_{CL}^{Fe\ 3p}\right)_{LFO/LNO}$, where E_{CL} is the chosen core level energy and E_v is the position of valence band maximum[32]. The core level and VBM binding energy difference is measured in LFO and LNO thin films, and the core level energy difference is measured in the heterostructure. The individual LFO (~6nm) and LNO (~3nm) thin films used to determine the core level and VBM energy difference for the band offset measurement. The Fe 3p and Ni 3p XPS regions are shown in Figure 3(d) and 3(e). Deconvolution of Fe 3p regions shows that there is an additional satellite peak along with $3p_{1/2}$ and $3p_{3/2}$. The Fe 3p spectra show essentially identical features for both the heterostructures and the thick LFO control sample, which is in

ACCEPTED MANUSCRIPT
Journal of Vacuum Science & Technology A
This is the author's peer reviewed, accepted manuscript. However, the online version of record will be different from this version once it has been copyedited and typeset.
PLEASE CITE THIS ARTICLE AS DOI: 10.1116/6.0002987

agreement with our interpretation of the DFT results above that indicated interfacial hole transfer would be orders of magnitude below the detection limit. Sensitivity to interfacial Fe in the 2 u.c. LFO film would be significant (~40% of the overall signal when accounting for attenuation through the surface layer), such that any features attributable to Fe^{4+} would be detected in our measurements.

Similarly, deconvolution of Ni 3p reveals multiple peaks that must be deconvolved under a consistent standard for analysis across samples[50]. The lowest Ni $3p_{3/2}$ feature (shaded region in red) was chosen as the LNO core level for E_{CL}^{LNO}. In order to maintain consistency in measurement between samples, the full width at half maximum, area ratio between spin-orbit split pairs, energy difference between various valence and spin multiplet peaks were constrained to be the same for all measurements. Differences in relative peak intensities between the heterostructure peaks in Figure 3(e) and the uniform LNO film in Figure 2(d) are small, suggesting that charge transfer was minimal and that the band alignment analysis is valid. The core level binding energies, VBM and VBO are presented in the Table 1. The VBO for both heterostructure samples are consistent with a value of ~0.3eV. Considering the error bar of at least 0.1 eV for these measurements with the XPS resolution, this is in good agreement with the VBO estimated from first-principles calculations.

TABLE I. Core level, VBM and band offset of LFO, LNO and LFO/LNO samples. The thickness of heterostructure samples: LFO/LNO-1 is 2uc/3uc and LFO/LNO-2 is 4uc/4uc. The energy values presented in the table are in eV.

Sample	Ni $3p^{3/2}$	Fe $3p^{3/2}$	VBM	ΔE_v

ACCEPTED MANUSCRIPT
Journal of Vacuum Science & Technology A
This is the author's peer reviewed, accepted manuscript. However, the online version of record will be different from this version once it has been copyedited and typeset.
PLEASE CITE THIS ARTICLE AS DOI: 10.1116/6.0002987

LFO	-	54.17	-0.2	
LNO	66.02	-	-1.1	
LFO/LNO-1	66.37	53.90	-0.65	0.28(0.1)
LFO/LNO-2	66.48	54.07	-0.70	0.33(0.1)

C. Electrocatalysis

Interfacial band engineering with epitaxial films can have a significant impact on functional properties, including electrocatalysis. To examine this impact, we studied the OER electrocatalysis using the epitaxial LFO/LNO thin film samples above. Films were converted into electrodes through back contact with a commercial glassy carbon disk and assembled into a rotating-disk shaft electrode. **Figure 4** shows the anodic scan for cyclic voltammetry data collected for each film at a scan rate of 20 mV s^{-1} while spinning the disk electrode at 2000 rpm to prevent bubble formation. Each voltammogram was collected following 25 continuous scans over the potential range 0.83 - 2.23 V vs RHE at 20 mV s^{-1}, starting at 0.83 V. The catalytic current densities observed at 1.6 V vs RHE (η_{OER}=370 mV) were found to be 26 μA cm^{-2} for LFO/LNO-1 and 55 μA cm^{-2} for LFO/LNO-2. The slightly larger current observed for LFO/LNO-2 may be due to the difference in thickness of the LFO or LNO layers. By comparison, the current density observed for a 5 u.c. LFO film (~2 nm) directly on an n-STO substrate (i.e. without an intermediate LNO layer) was recently reported by our groups to be 0.2 μA cm^{-2} [15]. This data is reprinted in **Figure 4** for direct comparison with the present LFO/LNO films.

ACCEPTED MANUSCRIPT
Journal of Vacuum Science & Technology A
This is the author's peer reviewed, accepted manuscript. However, the online version of record will be different from this version once it has been copyedited and typeset.
PLEASE CITE THIS ARTICLE AS DOI: 10.1116/6.0002987

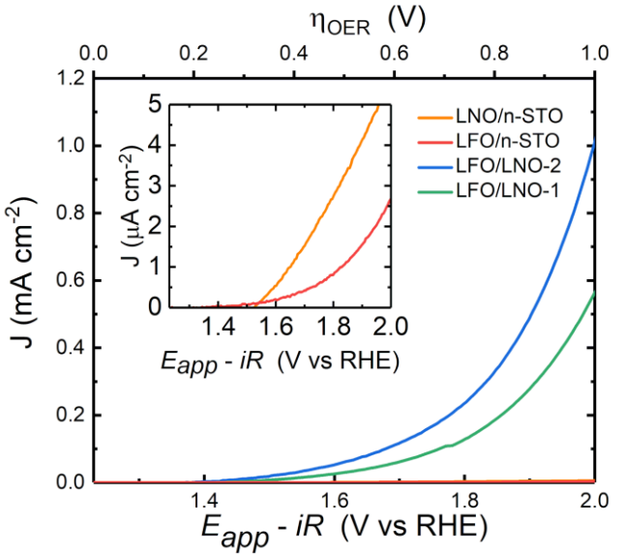

Figure 4: Anodic scans obtained from CV for LFO/LNO/n-STO films. Data collected in O2 saturated 0.1 M KOH aqueous electrolyte at 20 mV s^{-1} scan rate and 2000 rpm rotation. (Inset) Current density measured for 2 nm thick LFO film and 4 nm thick LNO film deposited directly on n-STO (LFO data taken from Burton et al[15])

IV. DISCUSSION

The two samples exhibit a 130-fold increase (LFO/LNO-1) and 275-fold increase (LFO/LNO-2) in catalysis observed for the LFO/LNO films compared to LFO alone is remarkable. We attribute this result to the interfacial hole doping due to the smaller VBO observed for the LFO/LNO interface (0.28-0.33 eV) than the LFO/STO interface reported previously (2.2 eV) and to the smaller energy gap between the LFO VBM and the Fermi level due to pinning from the LNO underlayer. The approximate band alignment diagram based on our experimental and theoretical determination of VBO based on our previous work[15] is summarized in Figure 5. Band bending shown in Figure 5(a) for LFO is a guide to the eye for expected behavior in thicker films due to the interfacial *p*-type doping from LNO. No measurements of band bending via XPS were made for these thin films. The

ACCEPTED MANUSCRIPT
Journal of Vacuum Science & Technology A
This is the author's peer reviewed, accepted manuscript. However, the online version of record will be different from this version once it has been copyedited and typeset.
PLEASE CITE THIS ARTICLE AS DOI: 10.1116/6.0002987

small *p*-type doping due to electrons transferred from LFO to LNO leave behind holes which move towards the surface (electrolyte-LFO interface) and contribute to water oxidation in the same fashion as holes produced by dopants in, for example, $(La,Sr)FeO_3$[31]. In $(La,Sr)FeO_3$, a ligand hole is hybridized between Fe cations and O anions[51] and serves as a catalyst for OER. Thus, creation of holes due the LFO/LNO interface will increase the surface oxidation kinetics, resulting in higher OER activity.

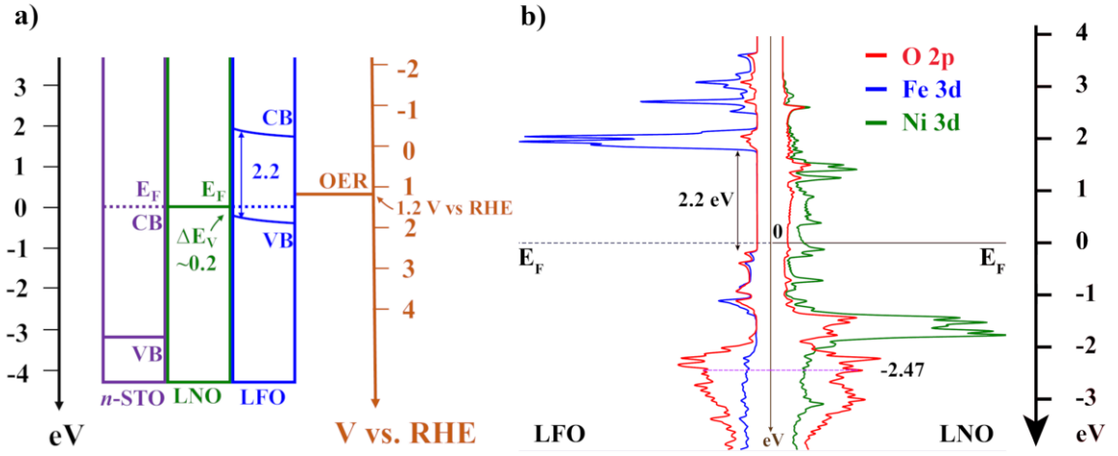

Figure 5: a) Experimental band alignment at STO/LNO/LFO interface b) Theoretical band alignment at LNO/LFO interface. Dashed line(magenta)at -2.47eV represents the O 2p band center at interfacial FeO_2 and NiO_2 layers.

We see that the VBM in LFO/LNO moves much closer to the OER activation energy (1.23V vs RHE) compared to the LFO/*n*-STO interface, reducing the overpotential significantly[15]. Moreover, during OER catalysis, electrons must travel from solution, through the valence band of LFO, and into the valence (conduction) band of LNO (*n*-STO). The band offset at the LFO/n-STO interface thus represents an uphill barrier for charge transfer. The insertion of LNO between STO and LFO thus decreases

ACCEPTED MANUSCRIPT
Journal of Vacuum Science & Technology A
This is the author's peer reviewed, accepted manuscript. However, the online version of record will be different from this version once it has been copyedited and typeset.
PLEASE CITE THIS ARTICLE AS DOI: 10.1116/6.0002987

this barrier significantly and results in greater electrocatalysis. Because both LNO and *n*-STO are metallic and the LFO films are of comparable thickness between samples (2-3 nm), the effects of conductivity from the underlying electrode are thought to be negligible in comparison to the changes in the band alignment for LFO, which shifts from *n*-type at the interface with *n*-STO to *p*-type at the interface with LNO. We also note that while the LNO layer is thinner than the typical thickness required for ideal metallic behavior[52], the LFO surface layer is likely to better preserve metallic conductivity, as has been observed for LaO-terminated LNO previously[53].

It is also noteworthy that we do not see evidence of significant formation of Fe^{4+} formal charge states based on either the DFT predictions or the XPS analysis of the interfaces. Previous analysis by Wang et al. of alloy La(Fe,Ni)O_3 thin films showed evidence of Fe^{4+} and Ni^{2+} formal charges in some samples with strongly enhanced electrocatalytic performance[24]. DFT models of these alloys also predicted formation of $Fe^{4-\delta}$ formal charge states at low Fe concentrations (12.5%) but did not use Hubbard *U* parameters to reproduce the experimental band gap of pure LFO[24]. While we do predict favorable hole transfer into LFO due to the small offset between the Fermi level pinned by LNO and the LFO valence, when accounting for the band gap of LFO in the model our analysis does not suggest that significant Fe^{4+} formal charge would be expected. Our result is in agreement with the DFT modeling performed by Yun et al. for Fe-doped LNO, which placed the Fe 3d electron < 0.5 eV below the Fermi level[30]. Further studies of LFO/LNO heterostructures using electron microscopy and X-ray absorption spectroscopy could help to address these open questions.

V. SUMMARY AND CONCLUSIONS

ACCEPTED MANUSCRIPT
Journal of Vacuum Science & Technology A
This is the author's peer reviewed, accepted manuscript. However, the online version of record will be different from this version once it has been copyedited and typeset.
PLEASE CITE THIS ARTICLE AS DOI: 10.1116/6.0002987

We have investigated the electronic structure of the epitaxial LFO/LNO interface theoretically and experimentally and related these insights to the strong OER activity of these heterostructures. Theoretical predictions indicate that the LFO VBM should lie ~0.2 eV below the Fermi level when pinned by an interface with LNO. Comparisons with experimental VBO measurements are in good agreement with these DFT predictions. We find that the OER activity of the heterostructure is much higher (~275 times for the best performing sample) when compared with the LFO and LNO thin films of same thicknesses. The small VBO offers low energy barriers for charge carriers and promotes electron transfer from the LFO valence band to LNO, leading to higher OER activity. This charge transfer is far below detectable levels from XPS, leaving Fe^{3+} and Ni^{3+} as the formal charges in LFO and LNO, respectively. Thus, our study highlights the importance of band engineering in developing a highly efficient OER catalyst without chemical doping or alloying.

SUPPLEMENTAL MATERIAL

See supplementary material at [URL will be inserted by AIP Publishing] for additional details on DFT modeling and carrier density estimation.

ACKNOWLEDGMENTS

R.P., A.R.B, B.H.F., and R.B.C. acknowledge support from the National Science Foundation (NSF) Division of Materials Research through grant NSF-DMR-1809847. Additionally, A.R.B. acknowledges support from the Alabama EPSCOR Graduate Research Scholars Program. M.A.K. acknowledges computational resources from the

ACCEPTED MANUSCRIPT
Journal of Vacuum Science & Technology A
This is the author's peer reviewed, accepted manuscript. However, the online version of record will be different from this version once it has been copyedited and typeset.
PLEASE CITE THIS ARTICLE AS DOI: 10.1116/6.0002987

Hopper HPC system at Auburn and funding support from NSF through NSF-DMR-1848344.

DATA AVAILABILITY

The data that support the findings of this study are available from the corresponding author upon request. Additional data is available in the supplementary material.

CONFLICTS OF INTEREST

The authors have no conflicts to disclose.

REFERENCES

[1] R. Comes, and S. Chambers, "Interface Structure, Band Alignment, and Built-In Potentials at $LaFeO_3$/n-$SrTiO_3$ Heterojunctions," Phys. Rev. Lett. **117**(22), 226802 (2016).

[2] S.A. Chambers, L. Qiao, T.C. Droubay, T.C. Kaspar, B.W. Arey, and P.V. Sushko, "Band Alignment, Built-In Potential, and the Absence of Conductivity at the $LaCrO_3$/$SrTiO_3$ (001) Heterojunction," Phys. Rev. Lett. **107**(20), 206802 (2011).

[3] S.A. Chambers, M.H. Engelhard, V. Shutthanandan, Z. Zhu, T.C. Droubay, L. Qiao, P.V. Sushko, T. Feng, H.D. Lee, T. Gustafsson, E. Garfunkel, A.B. Shah, J.-M. Zuo, and Q.M. Ramasse, "Instability, intermixing and electronic structure at the epitaxial $LaAlO_3$/$SrTiO_3$(001) heterojunction," Surface Science Reports **65**(10), 317–352 (2010).

[4] M.A. Kuroda, J. Tersoff, R.A. Nistor, and G.J. Martyna, "Optimal Thickness for Charge Transfer in Multilayer Graphene Electrodes," Phys. Rev. Applied **1**(1), 014005 (2014).

ACCEPTED MANUSCRIPT
Journal of Vacuum Science & Technology A
This is the author's peer reviewed, accepted manuscript. However, the online version of record will be different from this version once it has been copyedited and typeset.
PLEASE CITE THIS ARTICLE AS DOI: 10.1116/6.0002987

[5] A. Ohtomo, D.A. Muller, J.L. Grazul, and H.Y. Hwang, "Artificial charge-modulationin atomic-scale perovskite titanate superlattices," Nature **419**(6905), 378–380 (2002).

[6] A. Ohtomo, and H.Y. Hwang, "A high-mobility electron gas at the $LaAlO_3/SrTiO_3$ heterointerface," Nature **427**(6973), 423–426 (2004).

[7] I. González, S. Okamoto, S. Yunoki, A. Moreo, and E. Dagotto, "Charge transfer in heterostructures of strongly correlated materials," J. Phys.: Condens. Matter **20**(26), 264002 (2008).

[8] H. Chen, A.J. Millis, and C.A. Marianetti, "Engineering Correlation Effects via Artificially Designed Oxide Superlattices," Phys. Rev. Lett. **111**(11), 116403 (2013).

[9] J.E. Kleibeuker, Z. Zhong, H. Nishikawa, J. Gabel, A. Müller, F. Pfaff, M. Sing, K. Held, R. Claessen, G. Koster, and G. Rijnders, "Electronic Reconstruction at the Isopolar $LaTiO_3/LaFeO_3$ Interface: An X-Ray Photoemission and Density-Functional Theory Study," Phys. Rev. Lett. **113**(23), 237402 (2014).

[10] J. Garcia-Barriocanal, F.Y. Bruno, A. Rivera-Calzada, Z. Sefrioui, N.M. Nemes, M. Garcia-Hernández, J. Rubio-Zuazo, G.R. Castro, M. Varela, S.J. Pennycook, C. Leon, and J. Santamaria, "'Charge Leakage' at $LaMnO_3/SrTiO_3$ Interfaces," Advanced Materials **22**(5), 627–632 (2010).

[11] M.N. Grisolia, J. Varignon, G. Sanchez-Santolino, A. Arora, S. Valencia, M. Varela, R. Abrudan, E. Weschke, E. Schierle, J.E. Rault, J.-P. Rueff, A. Barthélémy, J. Santamaria, and M. Bibes, "Hybridization-controlled charge transfer and induced magnetism at correlated oxide interfaces," Nature Physics **12**(5), 484–492 (2016).

ACCEPTED MANUSCRIPT
Journal of Vacuum Science & Technology A
This is the author's peer reviewed, accepted manuscript. However, the online version of record will be different from this version once it has been copyedited and typeset.
PLEASE CITE THIS ARTICLE AS DOI: 10.1116/6.0002987

[12] A.S. Disa, D.P. Kumah, A. Malashevich, H. Chen, D.A. Arena, E.D. Specht, S. Ismail-Beigi, F.J. Walker, and C.H. Ahn, "Orbital Engineering in Symmetry-Breaking Polar Heterostructures," Phys. Rev. Lett. **114**(2), 026801 (2015).

[13] A. Prakash, N.F. Quackenbush, H. Yun, J. Held, T. Wang, T. Truttmann, J.M. Ablett, C. Weiland, T.-L. Lee, J.C. Woicik, K.A. Mkhoyan, and B. Jalan, "Separating Electrons and Donors in $BaSnO_3$ via Band Engineering," Nano Lett. **19**(12), 8920–8927 (2019).

[14] Z. Zhong, and P. Hansmann, "Band Alignment and Charge Transfer in Complex Oxide Interfaces," Phys. Rev. X **7**(1), 011023 (2017).

[15] A.R. Burton, R. Paudel, B. Matthews, M. Sassi, S.R. Spurgeon, B.H. Farnum, and R.B. Comes, "Thickness dependent OER electrocatalysis of epitaxial $LaFeO_3$ thin films," Journal of Materials Chemistry A **10**(4), 1909–1918 (2022).

[16] N.-T. Suen, S.-F. Hung, Q. Quan, N. Zhang, Y.-J. Xu, and H.M. Chen, "Electrocatalysis for the oxygen evolution reaction: recent development and future perspectives," Chem. Soc. Rev. **46**(2), 337–365 (2017).

[17] J. Xu, C. Chen, Z. Han, Y. Yang, J. Li, and Q. Deng, "Recent Advances in Oxygen Electrocatalysts Based on Perovskite Oxides," Nanomaterials **9**(8), 1161 (2019).

[18] J.R. Petrie, V.R. Cooper, J.W. Freeland, T.L. Meyer, Z. Zhang, D.A. Lutterman, and H.N. Lee, "Enhanced Bifunctional Oxygen Catalysis in Strained $LaNiO_3$ Perovskites," J. Am. Chem. Soc. **138**(8), 2488–2491 (2016).

[19] J. Suntivich, K.J. May, H.A. Gasteiger, J.B. Goodenough, and Y. Shao-Horn, "A Perovskite Oxide Optimized for Oxygen Evolution Catalysis from Molecular Orbital Principles," Science **334**(6061), 1383 (2011).

ACCEPTED MANUSCRIPT
Journal of Vacuum Science & Technology A
This is the author's peer reviewed, accepted manuscript. However, the online version of record will be different from this version once it has been copyedited and typeset.
PLEASE CITE THIS ARTICLE AS DOI: 10.1116/6.0002987

[20] J. Suntivich, W.T. Hong, Y.-L. Lee, J.M. Rondinelli, W. Yang, J.B. Goodenough, B. Dabrowski, J.W. Freeland, and Y. Shao-Horn, "Estimating Hybridization of Transition Metal and Oxygen States in Perovskites from O K-edge X-ray Absorption Spectroscopy," J. Phys. Chem. C **118**(4), 1856–1863 (2014).

[21] J. Rossmeisl, Z.-W. Qu, H. Zhu, G.-J. Kroes, and J.K. Nørskov, "Electrolysis of water on oxide surfaces," Journal of Electroanalytical Chemistry **607**(1), 83–89 (2007).

[22] I.C. Man, H.-Y. Su, F. Calle-Vallejo, H.A. Hansen, J.I. Martínez, N.G. Inoglu, J. Kitchin, T.F. Jaramillo, J.K. Nørskov, and J. Rossmeisl, "Universality in Oxygen Evolution Electrocatalysis on Oxide Surfaces," ChemCatChem **3**(7), 1159–1165 (2011).

[23] J. Bak, H.B. Bae, C. Oh, J. Son, and S.-Y. Chung, "Effect of Lattice Strain on the Formation of Ruddlesden–Popper Faults in Heteroepitaxial $LaNiO_3$ for Oxygen Evolution Electrocatalysis," J. Phys. Chem. Lett. **11**(17), 7253–7260 (2020).

[24] L. Wang, P. Adiga, J. Zhao, W.S. Samarakoon, K.A. Stoerzinger, S.R. Spurgeon, B.E. Matthews, M.E. Bowden, P.V. Sushko, T.C. Kaspar, G.E. Sterbinsky, S.M. Heald, H. Wang, L.W. Wangoh, J. Wu, E.-J. Guo, H. Qian, J. Wang, T. Varga, S. Thevuthasan, Z. Feng, W. Yang, Y. Du, and S.A. Chambers, "Understanding the Electronic Structure Evolution of Epitaxial $LaNi_{1-x}Fe_xO_3$ Thin Films for Water Oxidation," Nano Lett. **21**(19), 8324–8331 (2021).

[25] J. Low, J. Yu, M. Jaroniec, S. Wageh, and A.A. Al-Ghamdi, "Heterojunction Photocatalysts," Advanced Materials **29**(20), 1601694 (2017).

[26] J. Su, G.-D. Li, X.-H. Li, and J.-S. Chen, "2D/2D Heterojunctions for Catalysis," Advanced Science **6**(7), 1801702 (2019).

ACCEPTED MANUSCRIPT
Journal of Vacuum Science & Technology A
This is the author's peer reviewed, accepted manuscript. However, the online version of record will be different from this version once it has been copyedited and typeset.
PLEASE CITE THIS ARTICLE AS DOI: 10.1116/6.0002987

[27] X. Sun, D. Tiwari, and D.J. Fermin, "Promoting Active Electronic States in $LaFeO_3$ Thin-Films Photocathodes via Alkaline-Earth Metal Substitution," ACS Appl. Mater. Interfaces **12**(28), 31486–31495 (2020).

[28] L. Wang, K.A. Stoerzinger, L. Chang, J. Zhao, Y. Li, C.S. Tang, X. Yin, M.E. Bowden, Z. Yang, H. Guo, L. You, R. Guo, J. Wang, K. Ibrahim, J. Chen, A. Rusydi, J. Wang, S.A. Chambers, and Y. Du, "Tuning Bifunctional Oxygen Electrocatalysts by Changing the A-Site Rare-Earth Element in Perovskite Nickelates," Advanced Functional Materials **28**(39), 1803712 (2018).

[29] J. Bak, H. Bin Bae, and S.-Y. Chung, "Atomic-scale perturbation of oxygen octahedra via surface ion exchange in perovskite nickelates boosts water oxidation," Nat Commun **10**(1), 2713 (2019).

[30] T.G. Yun, Y. Heo, H. Bin Bae, and S.-Y. Chung, "Elucidating intrinsic contribution of d -orbital states to oxygen evolution electrocatalysis in oxides," Nat Commun **12**(1), 824 (2021).

[31] K. A. Stoerzinger, L. Wang, Y. Ye, M. Bowden, E. J. Crumlin, Y. Du, and S. A. Chambers, "Linking surface chemistry to photovoltage in Sr-substituted $LaFeO_3$ for water oxidation," Journal of Materials Chemistry A **6**(44), 22170–22178 (2018).

[32] S. Thapa, R. Paudel, M.D. Blanchet, P.T. Gemperline, and R.B. Comes, "Probing surfaces and interfaces in complex oxide films via in situ X-ray photoelectron spectroscopy," Journal of Materials Research **36**(1), 26–51 (2021).

[33] T. Peterlin-Neumaier, and E. Steichele, "Antiferromagnetic structure of $LaFeO_3$ from high resolution tof neutron diffraction," Journal of Magnetism and Magnetic Materials **59**(3), 351–356 (1986).

ACCEPTED MANUSCRIPT
Journal of Vacuum Science & Technology A
This is the author's peer reviewed, accepted manuscript. However, the online version of record will be different from this version once it has been copyedited and typeset.
PLEASE CITE THIS ARTICLE AS DOI: 10.1116/6.0002987

[34] J.L. García-Muñoz, J. Rodríguez-Carvajal, P. Lacorre, and J.B. Torrance, "Neutron-diffraction study of $RNiO_3$ (R=La,Pr,Nd,Sm): Electronically induced structural changes across the metal-insulator transition," Phys. Rev. B **46**(8), 4414–4425 (1992).

[35] P.E. Blöchl, "Projector augmented-wave method," Phys. Rev. B **50**(24), 17953–17979 (1994).

[36] J.P. Perdew, K. Burke, and M. Ernzerhof, "Generalized Gradient Approximation Made Simple," Phys. Rev. Lett. **77**(18), 3865–3868 (1996).

[37] J. Hubbard, "Electron Correlations in Narrow Energy Bands," Proceedings of the Royal Society of London. Series A, Mathematical and Physical Sciences **276**(1365), 238–257 (1963).

[38] K.J. May, and A.M. Kolpak, "Improved description of perovskite oxide crystal structure and electronic properties using self-consistent Hubbard U corrections from ACBN0," Phys. Rev. B **101**(16), 165117 (2020).

[39] H.J. Monkhorst, and J.D. Pack, "Special points for Brillouin-zone integrations," Phys. Rev. B **13**(12), 5188–5192 (1976).

[40] P. Giannozzi, S. Baroni, N. Bonini, M. Calandra, R. Car, C. Cavazzoni, D. Ceresoli, G.L. Chiarotti, M. Cococcioni, I. Dabo, A. Dal Corso, S. de Gironcoli, S. Fabris, G. Fratesi, R. Gebauer, U. Gerstmann, C. Gougoussis, A. Kokalj, M. Lazzeri, L. Martin-Samos, N. Marzari, F. Mauri, R. Mazzarello, S. Paolini, A. Pasquarello, L. Paulatto, C. Sbraccia, S. Scandolo, G. Sclauzero, A.P. Seitsonen, A. Smogunov, P. Umari, and R.M. Wentzcovitch, "QUANTUM ESPRESSO: a modular and open-source software

ACCEPTED MANUSCRIPT
Journal of Vacuum Science & Technology A
This is the author's peer reviewed, accepted manuscript. However, the online version of record will be different from this version once it has been copyedited and typeset.
PLEASE CITE THIS ARTICLE AS DOI: 10.1116/6.0002987

project for quantum simulations of materials," Journal of Physics: Condensed Matter **21**(39), 395502 (2009).

[41] E. Iguchi, and W. Hwan Jung, "Electrical Transports of $LaFe_{1-x}Ti_xO_3$ ($x \leq 0.10$)," J. Phys. Soc. Jpn. **63**(8), 3078–3086 (1994).

[42] S.R. Provence, S. Thapa, R. Paudel, T.K. Truttmann, A. Prakash, B. Jalan, and R.B. Comes, "Machine learning analysis of perovskite oxides grown by molecular beam epitaxy," Phys. Rev. Materials **4**(8), 083807 (2020).

[43] E.A. Kraut, R.W. Grant, J.R. Waldrop, and S.P. Kowalczyk, "Precise Determination of the Valence-Band Edge in X-Ray Photoemission Spectra: Application to Measurement of Semiconductor Interface Potentials," Phys. Rev. Lett. **44**(24), 1620–1623 (1980).

[44] R.B. Comes, P. Xu, B. Jalan, and S.A. Chambers, "Band alignment of epitaxial SrTiO3 thin films with $(LaAlO_3)_{0.3}$-$(Sr_2AlTaO_6)_{0.7}$ (001)," Applied Physics Letters **107**(13), 131601 (2015).

[45] S.A. Chambers, T. Droubay, T.C. Kaspar, and M. Gutowski, "Experimental determination of valence band maxima for $SrTiO_3$, TiO_2, and SrO and the associated valence band offsets with Si(001)," Journal of Vacuum Science & Technology B: Microelectronics and Nanometer Structures Processing, Measurement, and Phenomena **22**(4), 2205–2215 (2004).

[46] K. Gong, F. Xu, J.B. Grunewald, X. Ma, Y. Zhao, S. Gu, and Y. Yan, "All-Soluble All-Iron Aqueous Redox-Flow Battery," ACS Energy Lett. **1**(1), 89–93 (2016).

[47] A.J. Mao, H. Tian, X.Y. Kuang, J.W. Jia, and J.S. Chai, "Structural phase transition and spin reorientation of $LaFeO_3$ films under epitaxial strain," RSC Adv. **6**(102), 100526–100531 (2016).

ACCEPTED MANUSCRIPT
Journal of Vacuum Science & Technology A
This is the author's peer reviewed, accepted manuscript. However, the online version of record will be different from this version once it has been copyedited and typeset.
PLEASE CITE THIS ARTICLE AS DOI: 10.1116/6.0002987

[48] M.D. Scafetta, A.M. Cordi, J.M. Rondinelli, and S.J. May, "Band structure and optical transitions in $LaFeO_3$: theory and experiment," J. Phys.: Condens. Matter **26**(50), 505502 (2014).

[49] J. Varignon, M. Bibes, and A. Zunger, "Origin of band gaps in 3d perovskite oxides," Nat Commun **10**(1), 1658 (2019).

[50] L. Qiao, and X. Bi, "Direct observation of Ni^{3+} and Ni^{2+} in correlated $LaNiO_{3-\delta}$ films," (2011).

[51] M.A. Islam, Y. Xie, M.D. Scafetta, S.J. May, and J.E. Spanier, "Raman scattering in $La_{1-x}Sr_xFeO_{3-\delta}$ thin films: annealing-induced reduction and phase transformation," J. Phys.: Condens. Matter **27**(15), 155401 (2015).

[52] J. Fowlie, M. Gibert, G. Tieri, A. Gloter, J. Íñiguez, A. Filippetti, S. Catalano, S. Gariglio, A. Schober, M. Guennou, J. Kreisel, O. Stéphan, and J.-M. Triscone, "Conductivity and Local Structure of $LaNiO_3$ Thin Films," Advanced Materials **29**(18), 1605197 (2017).

[53] D.P. Kumah, A. Malashevich, A.S. Disa, D.A. Arena, F.J. Walker, S. Ismail-Beigi, and C.H. Ahn, "Effect of Surface Termination on the Electronic Properties of $LaNiO_3$ Films," Phys. Rev. Applied **2**(5), 054004 (2014).

Oulianov, R. A. Crowell, D. J. Gosztola, I. A. Shkrob, O. J. Korovyanko, and R. C. Rey-de-Castro, J. Appl. Phys. **101,** 053102 (2007).

[2]A. J. Elliot, "Rate constants and G-Values for the simulation of the radiolysis of light water over the range 0-300C," AECL Report No. 11073, Chalk River Laboratories, Chalk River, Ontario, Canada (1994).

ACCEPTED MANUSCRIPT
Journal of Vacuum Science & Technology A
This is the author's peer reviewed, accepted manuscript. However, the online version of record will be different from this version once it has been copyedited and typeset.
PLEASE CITE THIS ARTICLE AS DOI: 10.1116/6.0002987

[3]Y. Tabata, I. Itoh, and S. Tagawa, *CRC Handbook of Radiation Chemistry* (CRC Press, Boca Raton, 1991).

[4]Y. Young, *Physics in Today's World,* edited by A. Newman (Springer, New York, 1999), Vol. 2, pp. 62–68.

[5]J. Nelson, U.S. Patent No. 5,693,000 (12 December 2005).

[6]See supplementary material at [URL will be inserted by AIP Publishing] for [give brief description of material].

ACCEPTED MANUSCRIPT

Journal of Vacuum Science & Technology A

This is the author's peer reviewed, accepted manuscript. However, the online version of record will be different from this version once it has been copyedited and typeset.
PLEASE CITE THIS ARTICLE AS DOI: 10.1116/6.0002987

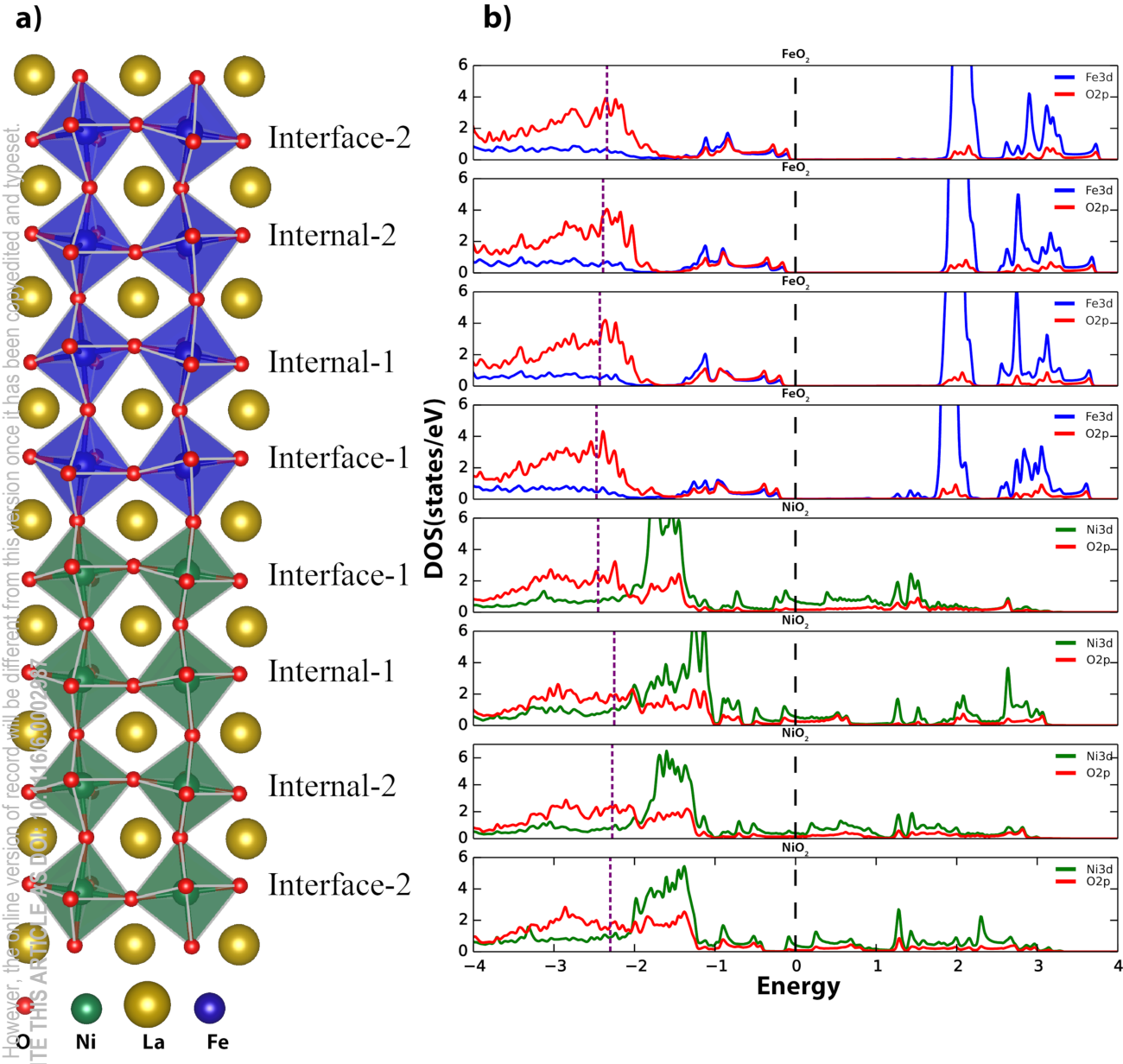

ACCEPTED MANUSCRIPT
Journal of Vacuum Science & Technology A
This is the author's peer reviewed, accepted manuscript. However, the online version of record will be different from this version once it has been copyedited and typeset.
PLEASE CITE THIS ARTICLE AS DOI: 10.1116/6.0001207

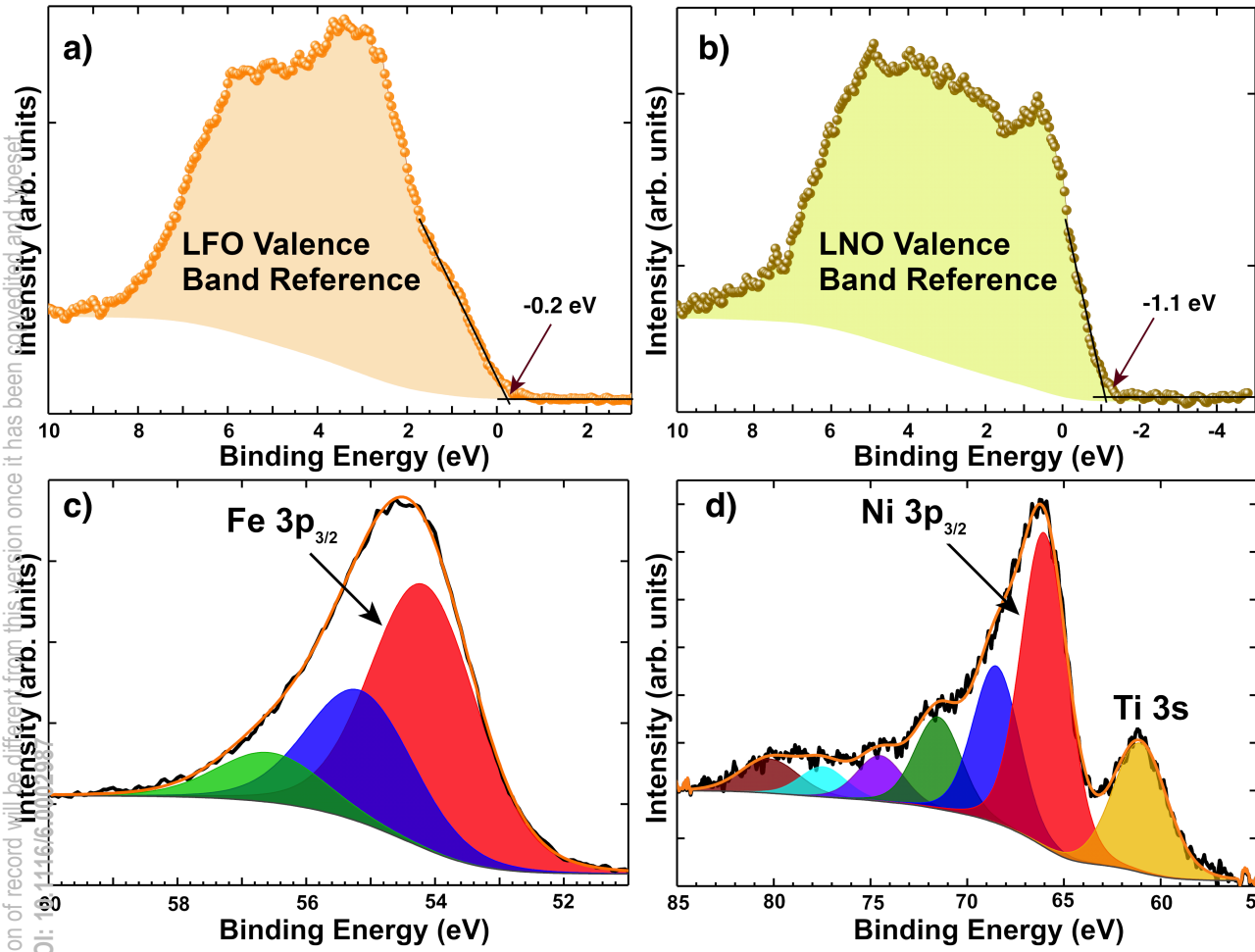

ACCEPTED MANUSCRIPT

Journal of Vacuum Science & Technology A

This is the author's peer reviewed, accepted manuscript. However, the online version of record will be different from this version once it has been copyedited and typeset.
PLEASE CITE THIS ARTICLE AS DOI: 10.1116/6.0002987

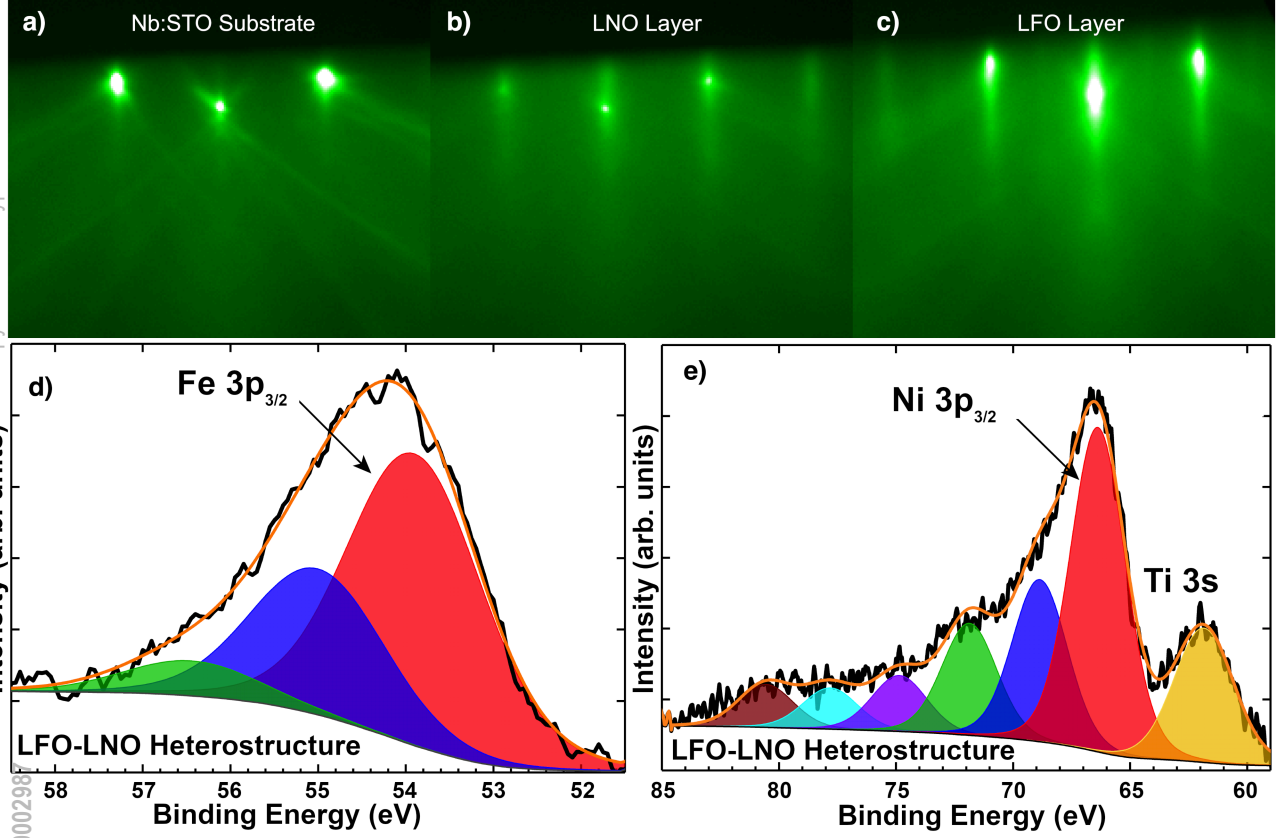

Journal of Vacuum Science & Technology A

ACCEPTED MANUSCRIPT

This is the author's peer reviewed, accepted manuscript. However, the online version of record will be different from this version once it has been copyedited and typeset.
PLEASE CITE THIS ARTICLE AS DOI: 10.1116/6.0002987

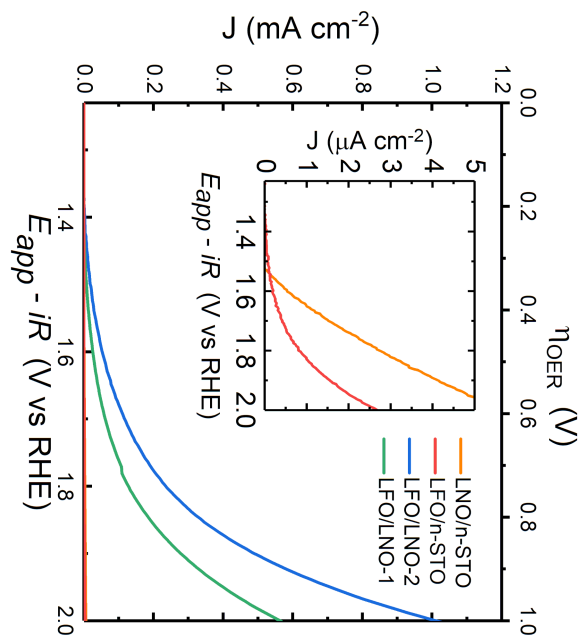

ACCEPTED MANUSCRIPT

Journal of Vacuum Science & Technology A

This is the author's peer reviewed, accepted manuscript. However, the online version of record will be different from this version once it has been copyedited and typeset.
PLEASE CITE THIS ARTICLE AS DOI: 10.1116/6.0002987